# Status of the Simbol-X detector background simulation activities

R. Chipaux[1,a)], U. Briel[2)], A. Bulgarelli[3)], L. Foschini[3)], E. Kendziorra[4)], C. Klose[5)], M. Kuster[5)], P. Laurent[1)] and C. Tenzer[4)]

***Simbol-X detector background simulation group***

**Abstract**

Using the Geant4 toolkit, a Monte-Carlo code to simulate the detector background of the Simbol-X focal plane instrument has been developed with the aim to optimize the design of the instrument. Structural design models of the mirror and detector satellites have been built and used as baseline for our simulations, to evaluate the different background contributions that must be taken into account to determine the sensitivity of the Simbol-X detectors. We work towards a simulation based background and mass model which can be used before and during the mission.

For different material compositions, material thicknesses, locations etc. the response of the instrument to the diffuse cosmic hard X-ray background and to the cosmic proton induced background have been calculated. As a result we present estimates of the background count rate expected in the low and high energy detector, and anti-coincidence rates. The effect of induced radioactivity in the detector and shielding materials and soft proton scattering in the mirror shells are also under study.

**Key words:** Simbol-X, Geant4, Monte-Carlo, cosmic rays.

Presented at the international workshop
*Simbol-X: the hard X-ray universe in focus*,
Bologna, Italy, May 14-16, 2007

[1)] CEA/DSM/Dapnia, CEA-Saclay, 91191 Gif sur Yvette Cedex, France

[2)] Max-Planck-Institut für extraterrestrische Physik, Giessenbachstrasse, 85748 Garching, Germany

[3)] Istituto di Astrofisica Spaziale e Fisica Cosmica, Via Gobetti 101, 40129 Bologna, Italy

[4)] Institut für Astronomie und Astrophysik, Universität Tübingen, Sand 1, 72076 Tübingen, Germany

[5)] Institut für Kernphysik, TU Darmstadt, Schlossgartenstrasse 9, 64289 Darmstadt, Germany

[a)] Corresponding author, email: remi.chipaux@cea.fr

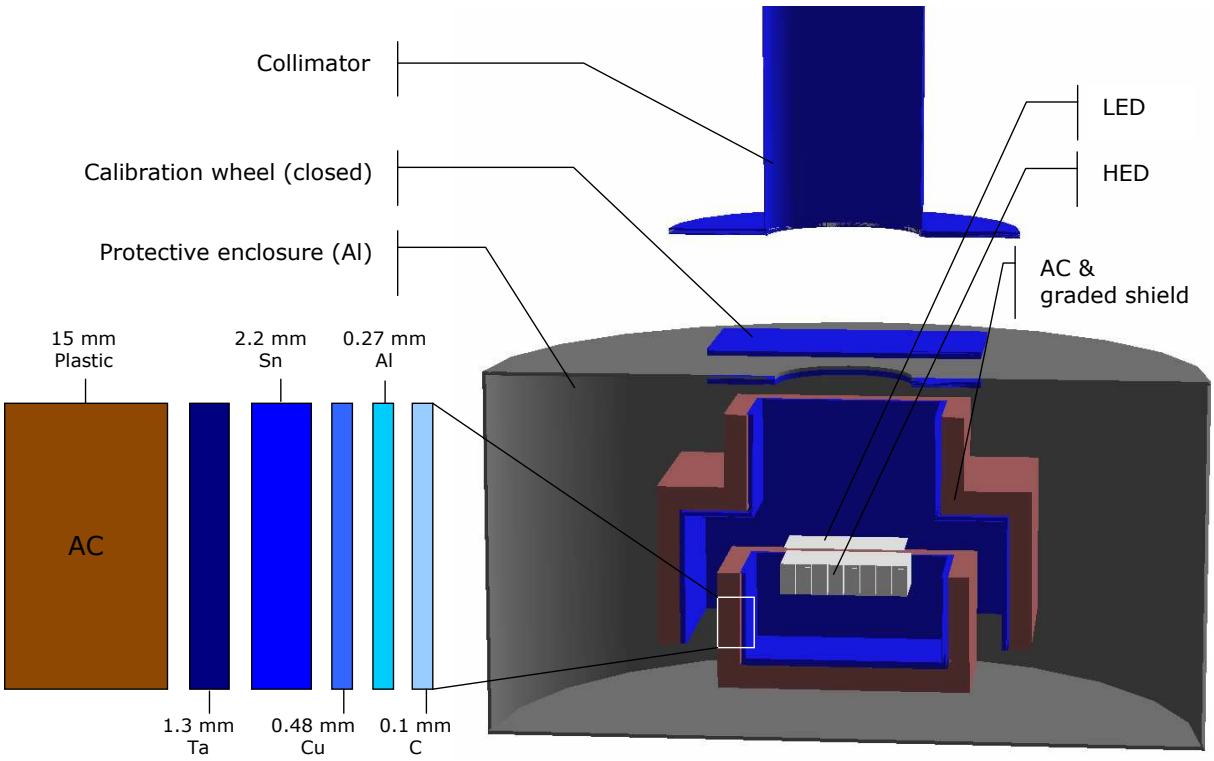


Figure 1: Mass model of the detectors, used for Geant4 Monte Carlo simulations.

# 1 Introduction

The focal plane detector of Simbol-X is made of two layers: a monolithic DEPFET Silicon detector is placed on top of a pixelized CdTe or CdZnTe detector. To achieve the scientific goals of the mission, an ambiguously low background level of below $10^{-4}$ counts $cm^{-2}s^{-1}keV^{-1}$ is required. This is far below the measured background of X-ray CCD cameras currently flown on missions like XMM-Newton and Chandra. The Monte-Carlo toolkit Geant4 is used by the Simbol-X background simulation group to optimize the design of the detector assembly in terms of low background. The background of the Simbol-X focal plane detector mainly stems from four components: the diffuse cosmic photon background, background induced by prompt interactions of high energy protons, a delayed component from induced radioactivity and soft protons funnelled by the telescope onto the detector. All four components are studied by our group in detail.

# 2 Simulations and models

## 2.1 Geant4

Geant4 is a toolkit for the simulation of the passage of photons and particles through matter. Its areas of application include high energy, nuclear and accelerator physics, as well as studies in medical and space science (Agostinelli et al. 2003; Allison et al. 2006).

In a preliminary study the model included only electromagnetic interactions (Tenzer 2006). In the work reported here hadronic interactions were added. In the work reported here the release 8.2.p01 of Geant4 was used and hadronic interactions were added. In addition the radioactive decay module of Geant4 was used for section 3.3, and the scattering of low energy protons module for section 3.4.

## 2.2 Simulation Models

### 2.2.1 Detectors

A model, shown in figure 1, of the current baseline configuration of the detector housing and the detectors has been built using Geant4 tools. This simplified geometry omits cables and some structures and details, but otherwise accurately reproduces the mechanical design as of January 2007. The central elements of the geometric model are the two detectors. The low-energy detector (LED) is represented by a slab of silicon, dimensions $80\times80\times0.45$ $mm^3$,

without segmentation. The high-energy detector (HED) is composed of $8 \times 8$ modules of cadmium zinc telluride ($Cd_{0.9}Zn_{0.1}Te$), $10 \times 10 \times 2$ mm$^3$, separated by 0.625 mm gaps. The segmentation of the HED is not yet used, the results presented refer to the sum of events in the 64 modules. The electronics associated to each module is represented by a $10 \times 10 \times 17.5$ mm$^3$ box in gold.

The detectors are surrounded by an anti-coincidence shield (AC), which consists of plastic scintillator slabs, 15 mm thick, divided in top, lateral and bottom parts to allow space for read-out connections. A graded shield is foreseen inside AC to reduce the incoming photon flux. It is designed to absorb all photons below 200 keV, leaving X-ray fluorescence below 0.3 keV and therefore below the detection limit of the LED (see figure 1 for details on the composition and thicknesses). An aluminum structure encloses and stabilizes the active parts of the camera.

A 1.6 m-long collimator sits above the aperture of the detector box to prevent photons coming from outside the field of view from hitting the detectors. It consists of the same materials as the graded shield. Its thickness, however, is decreasing with the distance from the detector to save weight and to maintain a constant effective thickness with respect to the incident angle of the incoming radiation.

A "calibration wheel", with the same structure as the graded shield, is placed between collimator and detector box. It allows us to either open or close the field of view. As a general rule, the cosmic photon-induced background is calculated with the field of view closed, the proton-induced one with the field of view open. Anyway, the wheel is practically transparent to cosmic protons. In the setup used here the spacecraft below the detector was not taken into account.

This model allows to estimate the effects of a change of materials, thicknesses or positioning on the detector background and thus helps to optimize the design of the detector system.

#### 2.2.2 Particle spectra and fluxes

The isotropic cosmic flux impinging the spacecraft is simulated by emitting particles from the inner surface of a sphere of radius larger than the spacecraft overall dimensions. To save computing time, the direction of emission is restricted to a cone containing the spacecraft.

In this study, we restrict ourselves to cosmic photon and proton fluxes, neglecting electrons and ions. The photon flux is supposed to follow the intensity and spectrum published by Gruber et al. (1999) for the diffuse cosmic hard X-rays. We extrapolate the analytic formula given by Gruber et al. down to 1 keV and take an upper limit equal to 100 MeV. In this range the integral of the X-ray flux is equal to 197.3 photons cm$^{-2}$s$^{-1}$ over $4\pi$. For the protons we use the spectrum computed by Claret (2006), at the expected launch date (near solar maximum), between 10 MeV and 100 GeV. In this range the integral of the proton flux is estimated to 2.31 protons cm$^{-2}$s$^{-1}$ over $4\pi$. As shown in figure 2, this spectrum is comparable to the spectra published by O'Gallagher and Maslyar III (1976) for different periods of the solar cycle.

#### 2.2.3 Optics

Concerning the mirror, the model is derived at the present state from the one developed for XMM (Nartallo 2002). As shown on figure 3, the optics is composed of 58 shells at 20 m from the detectors.

# 3 Results

## 3.1 Detector efficiency

We performed simulations of the on-axis efficiency of the two detectors. It has been obtained by simulating an on-axis source 3 m distant from the LED along the $z$ axis and generating a monochromatic beam of 1000 photons for each energy (5, 10, 15, 20, 25, 30, 40, 50, 70, 100 keV). Results are reported on figure4. AC vetoing was not taken into account but anyway negligible.

## 3.2 Detectors prompt background

As shown in figure 5 and reported in table 1, in the current setup the background count rates are dominated by the cosmic protons. The cosmic photons induce a count rate of about $10^{-4}$ counts cm$^{-2}$s$^{-1}$keV$^{-1}$ in LED and 3 $10^{-4}$ in HED. As expected, the AC is not efficient in that case. The cosmic protons induce a much higher background,

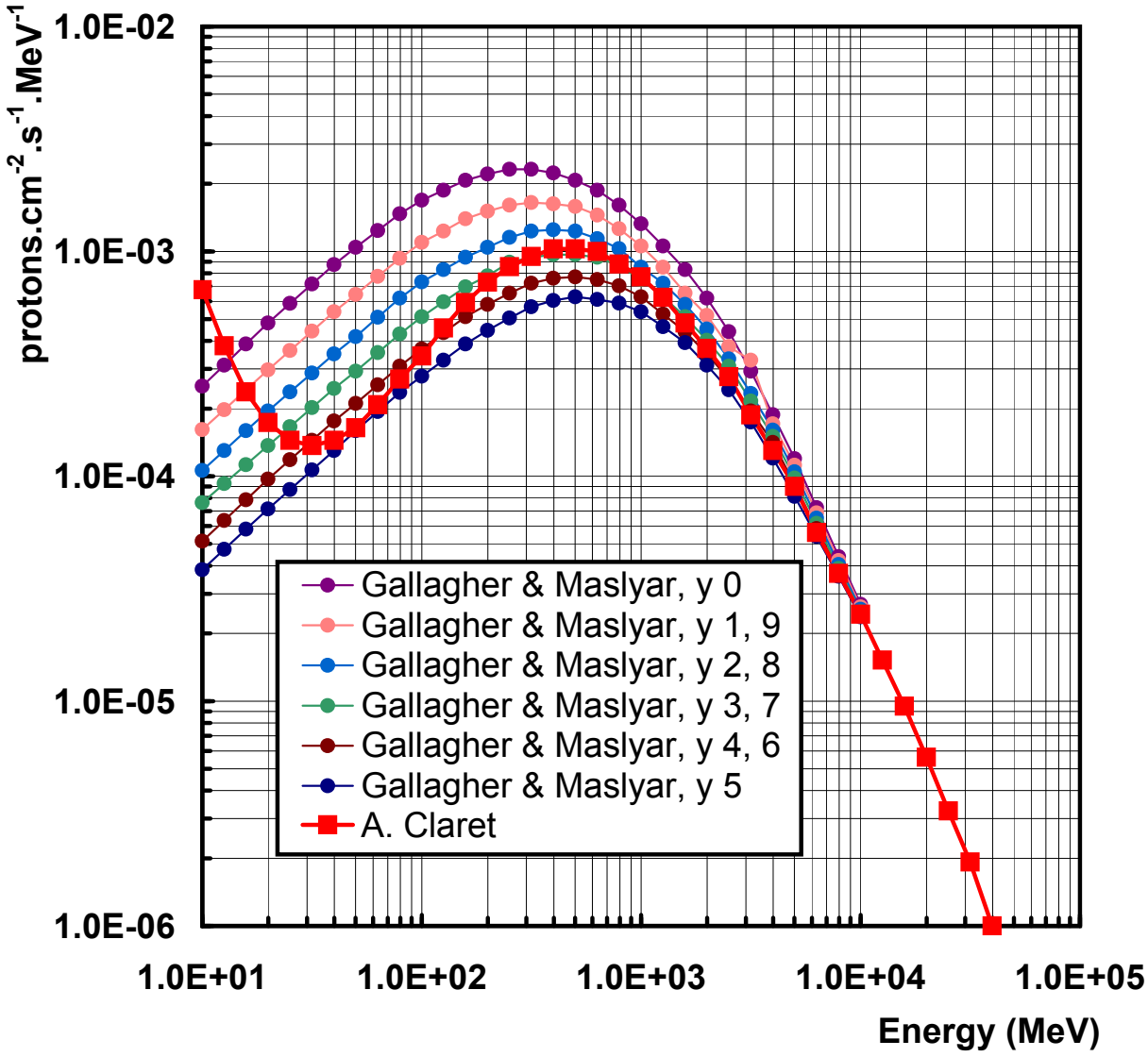


Figure 2: Proton spectrum calculated by Claret (2006) (squares), as used in the present simulation. For comparison, the spectra published by O'Gallagher and Maslyar III (1976) for different periods of the solar cycle are also shown.

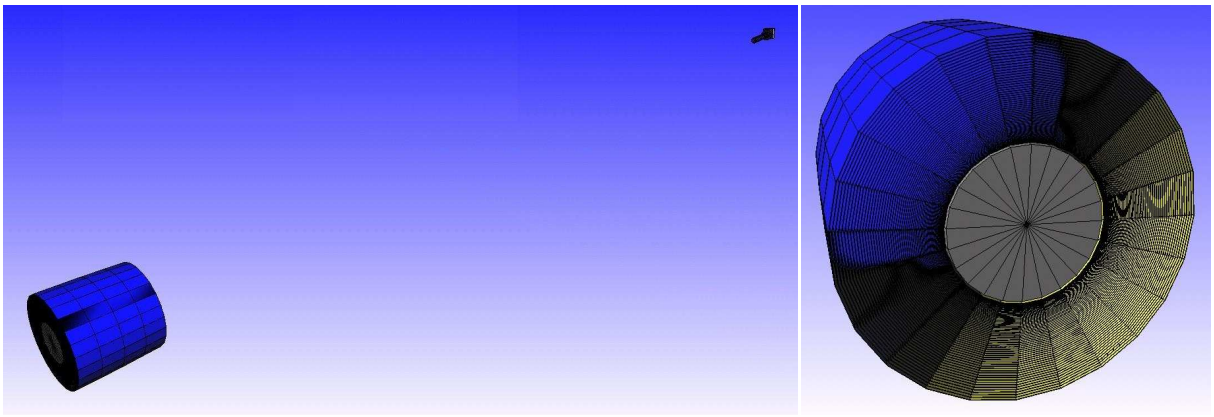

Figure 3: Monte Carlo model of the mirror.

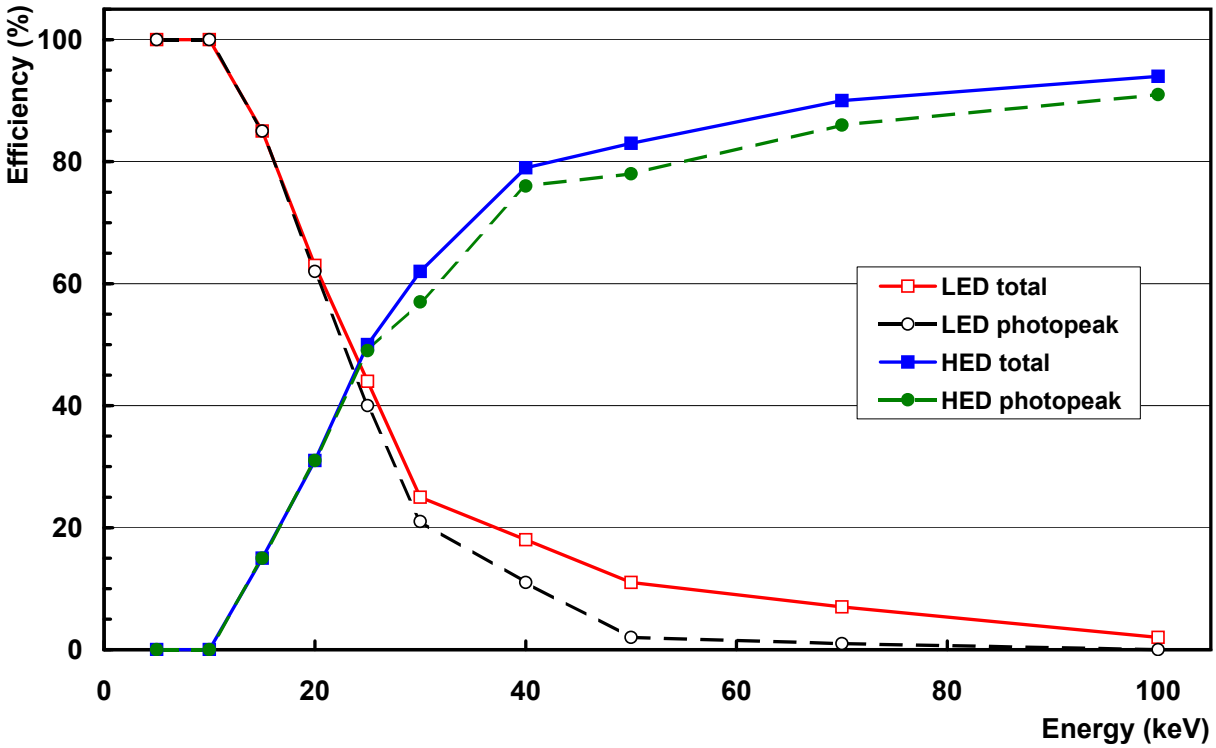


Figure 4: Detectors efficiencies in the scientifically useful energy band.

Table 1: Count rates (in $10^{-5}$ counts $cm^{-2}s^{-1}keV^{-1}$) in LED and HED due to cosmic photons and protons for various configurations of AC: a) basic setup with AC made of plastic scintillator; b) AC made of NaI; c) same as a) but protective enclosure in Ta instead of Al. d) same as b) but protective enclosure in Ta instead of Al.

| | AC off | AC on |
|---|---|---|
| a) AC plastic | | |
| photons; LED | 9.5 ± 0.9 | 9.2 ± 0.9 |
| photons; HED | 33 ± 1 | 32 ± 1 |
| protons; LED | 271 ± 3 | 14 ± 1 |
| protons; HED | 316 ± 2 | 9.0 ± 0.2 |
| b) AC NaI | | |
| photons; LED | 7.5 ± 1.3 | 6.9 ± 1.2 |
| photons; HED | 23.3 ± 1.1 | 21.5 ± 1.1 |
| protons; LED | 331 ± 3 | 13 ± 1 |
| protons; HED | 428 ± 2 | 9.9 ± 0.3 |
| c) AC plastic + Ta box | | |
| photons; LED | 2.3 ± 0.5 | 2.2 ± 0.5 |
| photons; HED | 9.9 ± 0.5 | 9.1 ± 0.5 |
| protons; LED | 322 ± 13 | 15 ± 3 |
| protons; HED | 395 ± 7 | 12 ± 2 |
| d) AC NaI + Ta box | | |
| photons; LED | 2.5 ± 0.5 | 1.4 ± 0.4 |
| photons; HED | 7.6 ± 0.4 | 6.1 ± 0.4 |
| protons; LED | 373 ± 8 | 15 ± 2 |
| protons; HED | 531 ± 5 | 16 ± 1 |

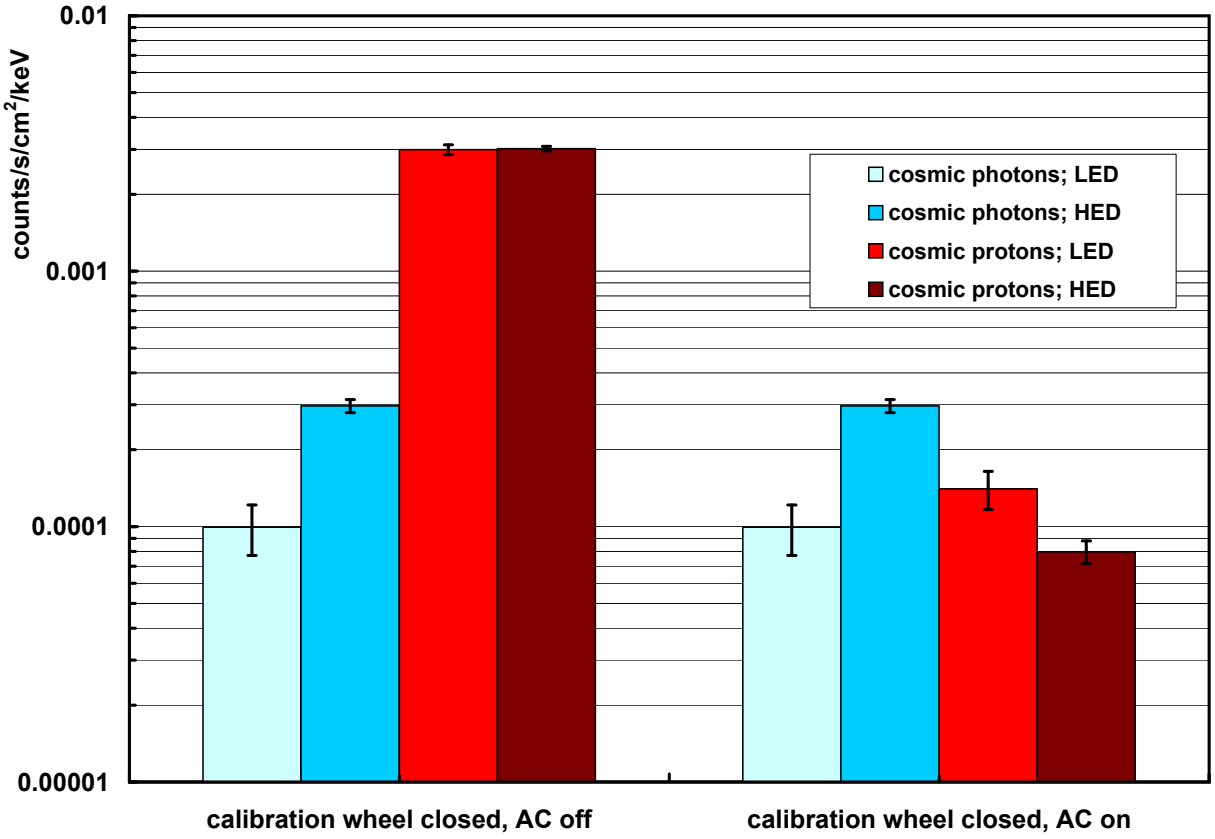


Figure 5: Count rates in the detectors due to cosmic photons and protons. Left: AC not active, right: AC active, threshold 100 keV.

in the range of about 3 $10^{-3}$ counts $cm^{-2}s^{-1}keV^{-1}$ in both detectors. The AC plays here its full role and allows reduction of the effective proton background to the range of $10^{-4}$ counts $cm^{-2}s^{-1}keV^{-1}$.

The total background count rate is in the range of 2 $10^{-4}$ counts $cm^{-2}s^{-1}keV^{-1}$ in LED and twice as much in HED.

Some ways to reduce it are proposed and under study, among them: - to replace the plastic scintillator in AC by a crystal such as NaI, CsI or $LaBr_3$; - to increase the thickness of the tantalum shield in order to increase the shielding power against photons. However, this leads to an increase of the mass of material, and consequently of the number of proton interactions and count rates. The first results with a NaI AC, shown on figure 6, indicate only a slight improvement of the photon-induced background, counterbalanced by a small increase of the proton-induced background. A study with the higher density scintillators $LaBr_3$ is in progress.

Increasing the tantalum thickness in the graded shield to 3 mm reduces the photon-induced part of the background on the HED by 25 %. However, as shown by figure 7, the thicker material layer gives rise to a higher background due to protons, resulting in a higher total detector background. However, these additional events are almost entirely tagged by AC.

An alternative could be to place this supplementary tantalum shield outside of the AC. A preliminary study with a setup where the 2.3 mm thick aluminum of the protective enclosure was replaced by tantalum shows that it has a large effect on the photon-induced background: A reduction by a factor 5 in LED and 3 in HED is observed, as shown in table 1 and figure 8, to be compared with the 25 % reduction obtained by an increase of the tantalum thickness of the internal graded shield, while the effect on the proton-induced background remains more or less the same. This may indicate that the present mechanical setup suffers from indirect leaks. Optimization of the shielding geometry should be done to suppress these leaks. One should note that the spacecraft, which is sitting below the detector box, will also act as a shield.

As indicated in figure 9, the count rate in AC due to cosmic protons ranges around 6 kHz, resulting in a large dead time of the LED, not easily sustainable by this detector. If one considers only the upper part of the AC ("top" curve in the figure), the count rate decreases only to ≈5.5 kHz. Other schemes could however be considered to decrease rate and dead time: different AC segmentation, optimization of the veto procedure, (for example using correlation between LED, HED and AC) etc.

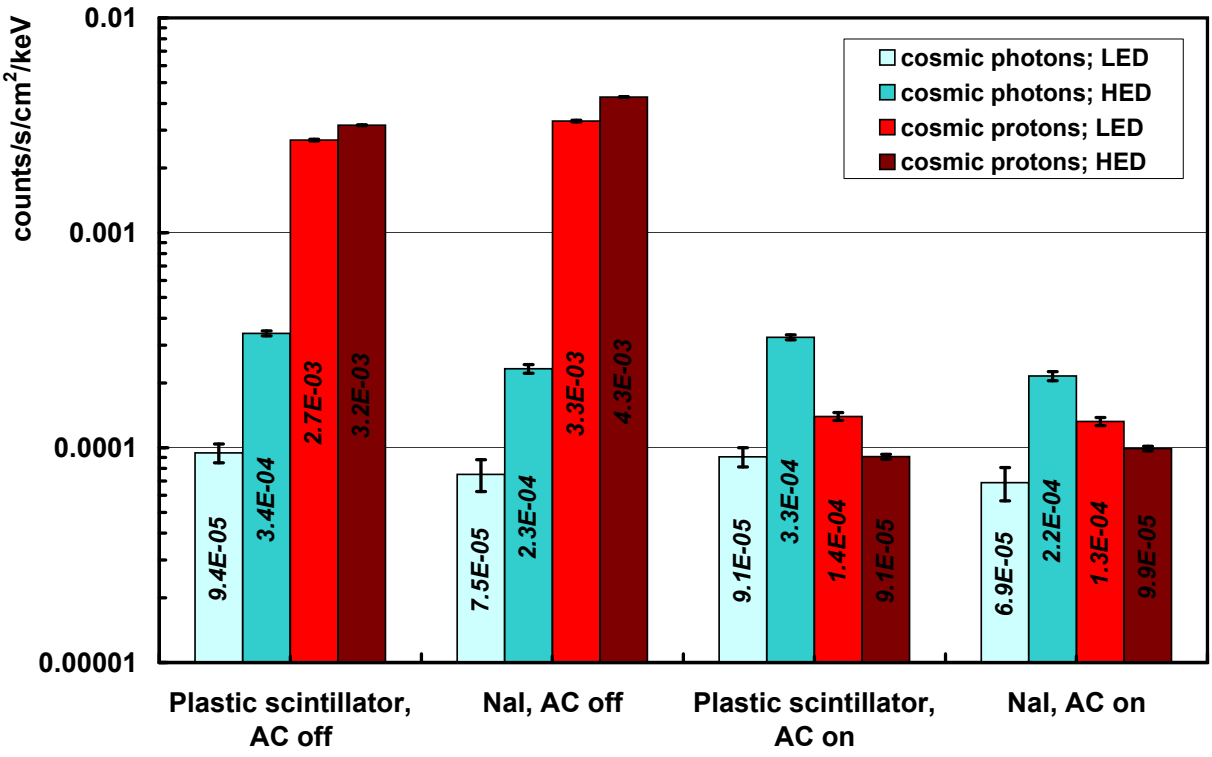


Figure 6: Comparison of count rates in the detectors due to cosmic photons and protons for two materials of the AC shield: plastic scintillator and NaI. Left: AC not active; right: AC active, threshold 100 keV.

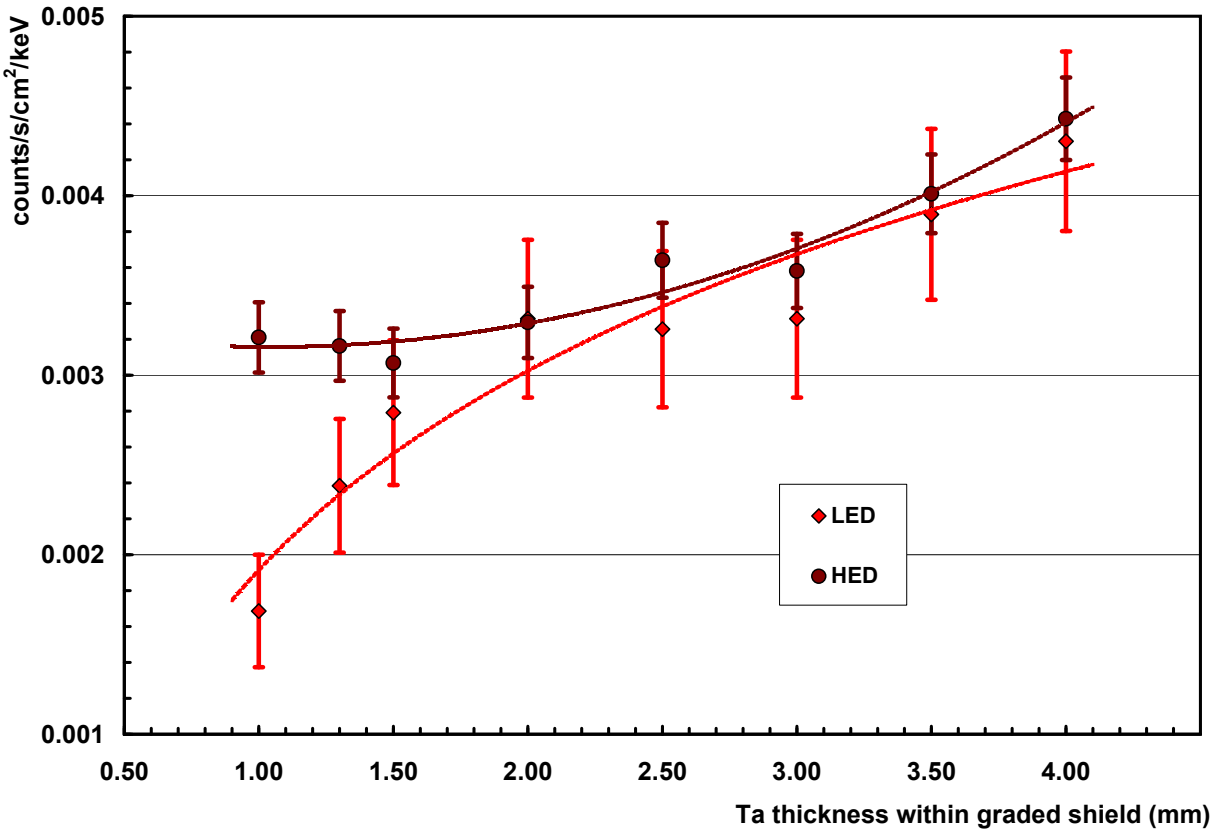


Figure 7: Variation of the count rates in detectors due to cosmic protons as function of the tantalum thickness in graded shield. The nominal thickness is 1.3 mm. The solid lines are guides for the eyes.

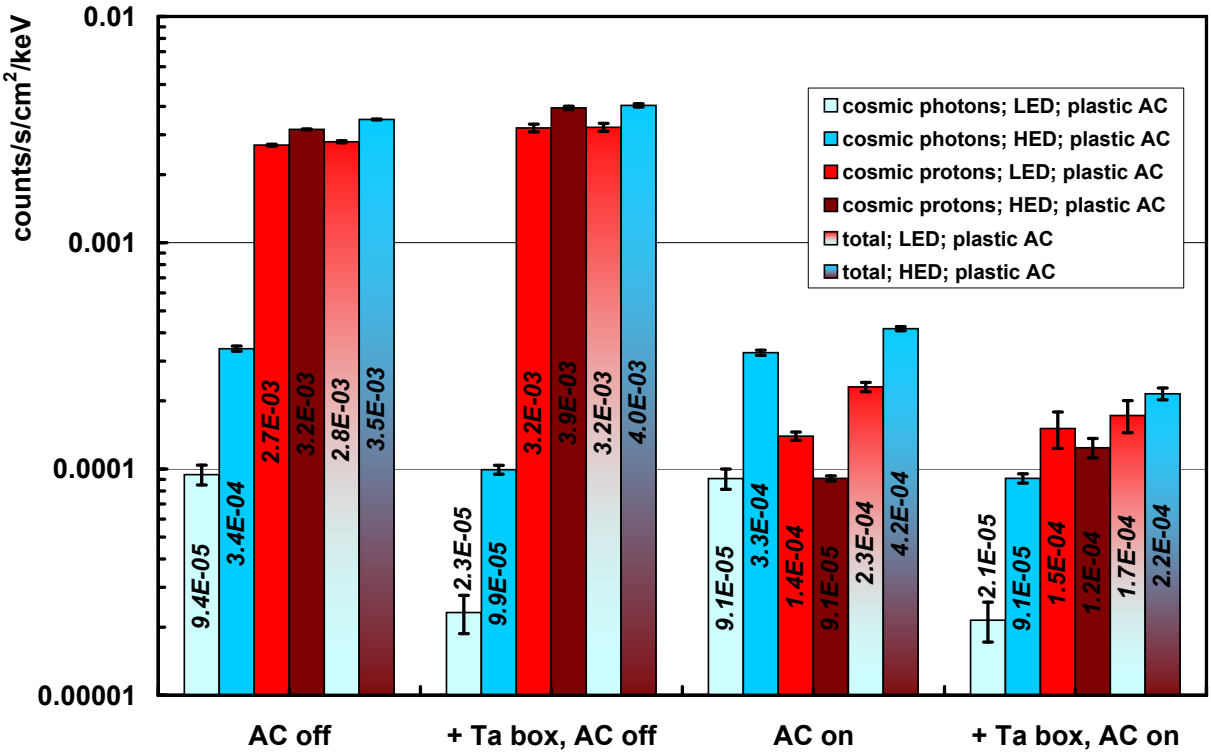


Figure 8: Comparison of count rates in the detectors due to cosmic photons and protons for the basic setup and the same setup where the material of the protective enclosure box (Al) has been replaced by Ta. Left: AC not active, right: AC active, threshold 100 keV.

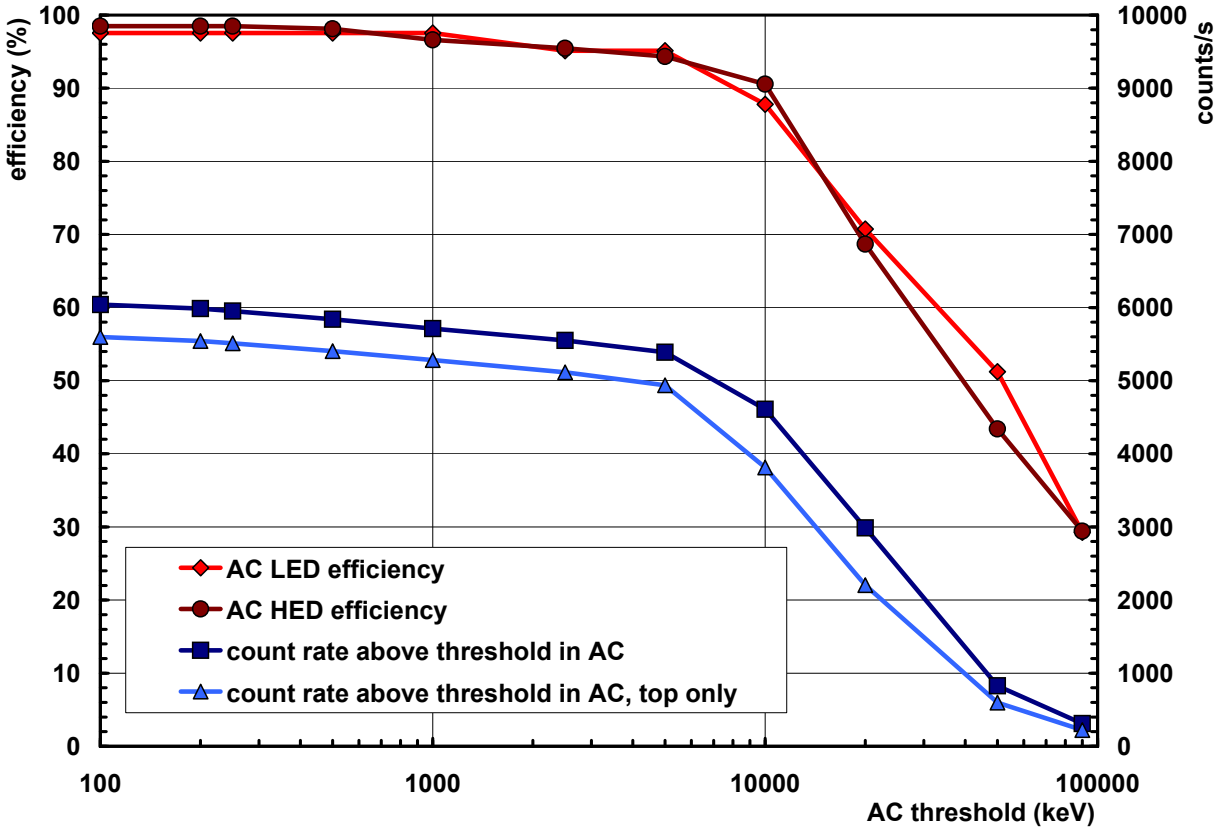


Figure 9: AC (plastic) performance (left scale) and count rates (right scale) resulting from cosmic protons as function of the AC threshold.

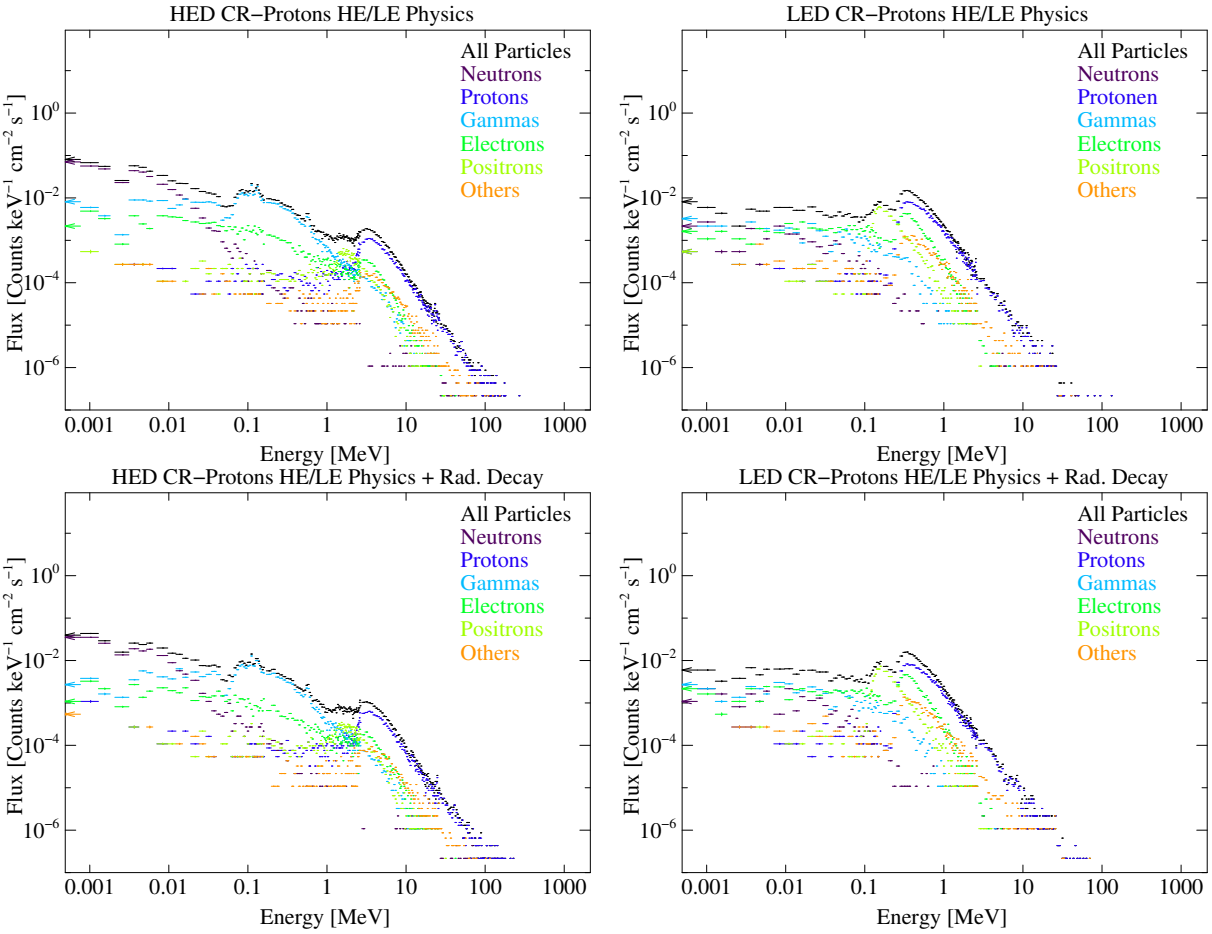


Figure 10: Energy deposition spectra due to cosmic protons in LED (right) and HED (left) with (down) or without (up) radioactive decay.

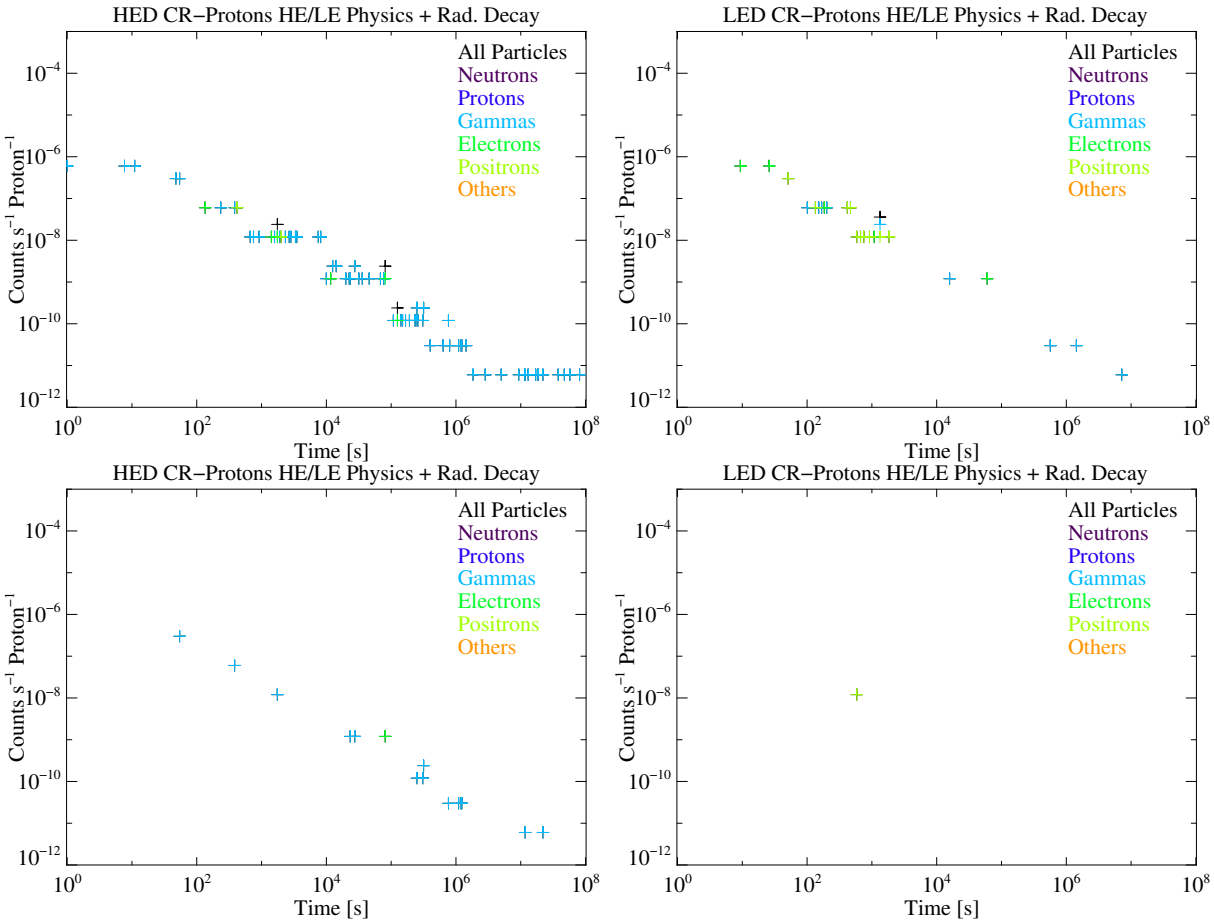


Figure 11: Variation in time of the delayed background in LED (right) and HED (left). Up: all events; down: events with energy in the detection ranges.

Table 2: Flux of the delayed background component (in $10^{-5}$ counts $cm^{-2}s^{-1}keV^{-1}$) for the HED and the LED.

| | Flux | | Fractional contribution | |
|---|---|---|---|---|
| t ≥ | LED | HED | LED | HED |
| 10 s | 2.92 ± 2.06 | 5.69 ± 1.31 | 0.5 % | 0.7 % |
| $10^2$ s | 2.92 ± 2.06 | 5.39 ± 1.27 | 0.5 % | 0.7 % |
| $10^4$ s | 1.46 ± 1.46 | 4.79 ± 1.20 | 0.3 % | 0.6 % |
| $10^6$ s | 1.46 ± 1.46 | 2.40 ± 0.85 | 0.3 % | 0.3 % |
| $10^8$ s | 1.46 ± 1.46 | 0.90 ± 0.52 | 0.3 % | 0.1 % |

Table 3: Activation of differents parts of the Symbol-X geometry. The activation parts are relative to the total number of all decay events produced in the detector geometry.

| Part | Fraction of activation |
|---|---|
| Ta-shield | 64.9 % |
| AC-shield | 11.1 % |
| Electronic module | 8.6 % |
| Sn-shield | 6.5 % |
| Protective enclosure | 5.1 % |
| HED module | 1.4 % |

### 3.3 Induced radioactivity

Radioactivity induced in the spacecraft by cosmic rays leads to delayed background in the detectors. First results indicate that the contribution of the delayed background to the overall background is of the order of 0.5 %, (see table 2 and figures 10 and 11). However, radioactivation is very dependent on materials and their locations, (see for example table 3), and thus would be more precisely evaluated with a more detailed and realistic mass model of the spacecraft.

### 3.4 Optics

A preliminary analysis of the energy deposit of 500 keV protons scattered into the mirror shells has been performed. About $10^6$ protons have been randomly generated over the surface of an annular source on top of the shells, with a source half-angle of 0.5 degrees. The detector spacecraft has been divided into collimator, structure (called S/C in figure12), LED, HED and AC, and energy deposits in these different parts were recorded. The results, shown in figure 12, indicate that, with the generated statistic, no protons or secondary reaches the HED.

## 4 Conclusions

Our Geant4 simulations have shown that an active anticoincidence around the detectors is absolutely required to achieve a background level of the order of $10^{-4}$ counts $cm^{-2}s^{-1}keV^{-1}$. It has thus become apparent that the present design should be optimized toward a more compact and above all hermetic coverage of the detectors by the AC. However, in the same time, different schemes should be actively studied to decrease AC count rate and LED dead time. At this preliminary state of study, neither the induced radioactivity nor the scattering of soft protons in the optics do seem to be a major problem compared to the prompt background.

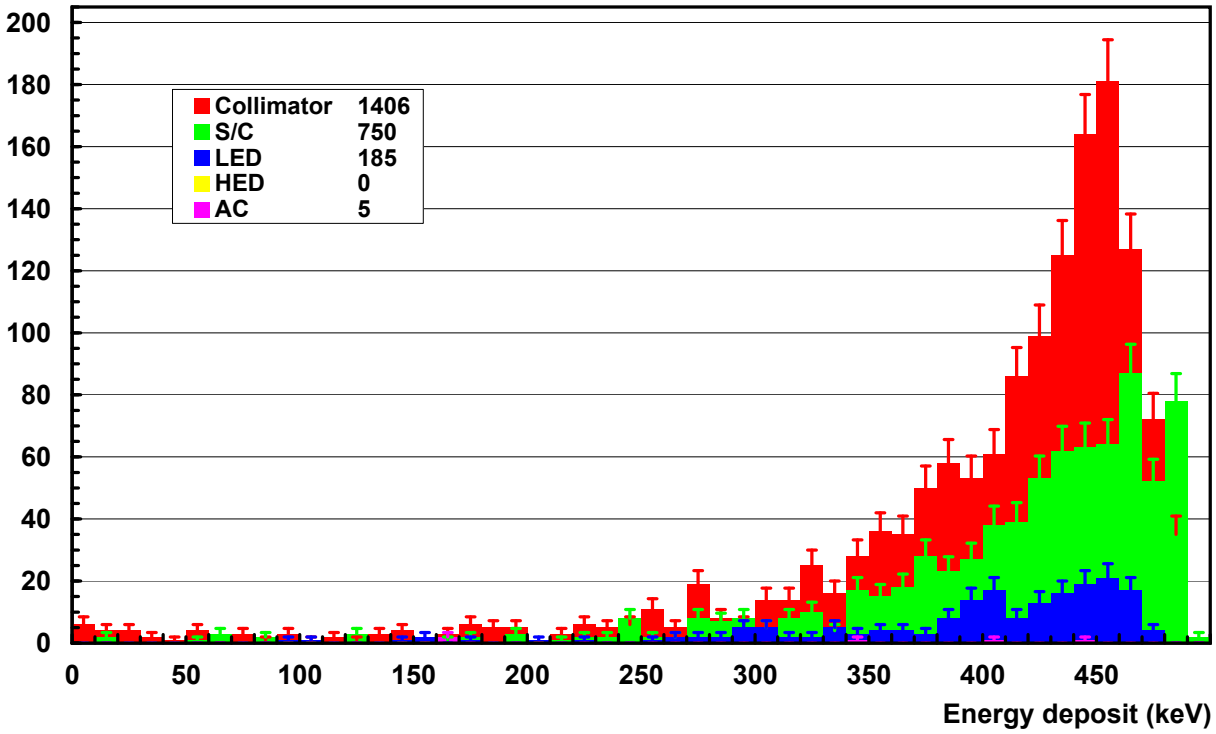


Figure 12: Energy deposit in LED, HED, AC, collimator and structure (S/C) for 500 keV protons scattered in the mirror shells.

**Acknowledgements**

This work was partly supported by Bundesministerium für Wirtschaft und Technologie through Deutsches Zentrum für Luft- und Raumfahrt e.V. (DLR) grants FKZ 50QR0601 and FKZ 50OG0601.

# References

Agostinelli S. et al., "Geant4 a simulation toolkit", Nucl. Instrum. and Meth. A 506 (2003) 250-303.

Allison J. et al., "Geant4 developments and applications", IEEE Trans. Nucl. Sci 53 (2006) 270-278.

Claret A., "Space environment of Simbol-X", CEA/Dapnia/SAp internal report, 2006.

Gruber D.E. et al., "The spectrum of diffuse cosmic hard X-rays measured with HEAO 1", The Astrophysical Journal, 520 (1999) 124.

Nartallo R., "The propagation of low-energy protons through the XMM-Newton optics", Esa/estec/tos-ema/02-067/RN, Issue 1, revision 0;
`http://space-env.esa.int/Feedback.htm?document=ProjectSupport/XMMNewton/tos-em-02-067.pdf`

O'Gallagher J.J. and Maslyar III G.A., "A dynamic model for the time evolution of the modulated cosmic ray spectrum", J. Geophys. Res. 81 (1976) 1319.

Tenzer C. et al., "Monte Carlo simulations of stacked X-ray detectors as designed for Simbol-X", Proc. SPIE 6266 (2006) 626620.